Soft Matter

Dynamic Article Links

Cite this: *Soft Matter*, 2012, **8**, 11933

www.rsc.org/softmatter

PAPER

Diffusive dynamics of nanoparticles in aqueous dispersions†

Kai He, Melissa Spannuth, Jacinta C. Conrad* and Ramanan Krishnamoorti*

Received 15th June 2012, Accepted 12th September 2012
DOI: 10.1039/c2sm26392k

The diffusive dynamics of 100 nm to 400 nm diameter polystyrene nanoparticles dispersed in water were studied using brightfield and fluorescence based differential dynamic microscopy (DDM) and compared to those obtained from dynamic light scattering. The relaxation times measured with brightfield and fluorescence DDM over a broad range of concentration of nanoparticles ($10^{-6} \leq \varphi \leq 10^{-3}$) and scattering vectors ($0.5\ \mu m^{-1} < q < 10\ \mu m^{-1}$) are in excellent agreement with each other and extrapolate quantitatively to those obtained from DLS measurements. The diffusion coefficients extracted from the q-dependent relaxation times using all three methods are independent of the nanoparticle concentration.

1. Introduction

Understanding the diffusion and transport of nanoscale particles in complex and confined geometries and fluids is of significant interest for many chemical, biological and physical systems. For instance, the targeted delivery of cancer drugs encapsulated in nanoparticles requires their transport through tissue prior to binding to the cancerous cells.[1] Similarly, the fate of nanoparticles in soil and their potential accumulation in ground water sources has become a significant toxicological concern.[2] Two complementary techniques have been employed to investigate the structure and dynamics of these and similar nanoparticle systems: radiation scattering based on incident light, X-rays and neutrons and direct space light microscopy measurements.[3–6] Traditionally, the diffusive dynamics of particles in dilute suspensions have been measured using dynamic light scattering (DLS). However, DLS is typically not reliable for measuring dynamics in complex geometries or at high concentrations of particles, although the recent development of DLS microscopy has allowed these methods to be applied to biological samples.[7,8] Conversely, particle-tracking algorithms applied to a time series of real-space micrographs[6,9] yield trajectories of individual particles and thereby have provided significant understanding of the dynamics of micron-sized particles and bacteria.[10,11] However, particle-tracking methods become more challenging for nanoparticles as the size of the objects is often smaller than the resolution of the microscope. Surmounting these limitations imposed by particle-tracking methods and by traditional and microscopic DLS therefore requires new approaches to measure the diffusive dynamics of nanoparticles, especially in complex media.

Recently, Cerbino and coworkers have developed a technique termed differential dynamic microscopy (DDM) that uses a standard optical microscope, a white light source and a video camera to examine the dynamics of particles both below the resolution limit of the microscope (70 nm) and above it (420 nm) in a viscous medium.[12,13] Briefly, this technique analyzes the intensity fluctuations in a time series of microscopy images in Fourier space to obtain information similar to DLS but at a lower range of scattering wave vectors. Wilson *et al.* applied the DDM methodology to living systems by examining the dynamics of swimming bacteria using brightfield DDM.[14] Also Reufer *et al.* extended the use of DDM to probe the dynamics of anisotropic particles and extract their orientational order parameter.[15] Extending DDM to analyze the signal from fluorescent particles[16] and using confocal microscopy[17] have allowed DDM to be used in complex environments, including conditions where scattering from different moieties can render brightfield DDM hard to interpret, and in suspensions at higher concentration of particles. The combination of brightfield and fluorescence DDM (b-DDM and f-DDM, respectively) as probes for nanoparticle dynamics, especially over a broad range of particle concentrations, appears to therefore provide a convenient and relatively inexpensive route for characterizing the dynamics of nanoparticles in complex environments. However, b-DDM and f-DDM intrinsically probe different optical responses of the system that in turn are significantly different from the DLS measurements. We thus seek in this paper to establish the equivalence of brightfield DDM, fluorescence DDM, and DLS methods for particles over a size range spanning the resolution limit of optical microscopy, and thereby demonstrate the use of DDM-based methods to quantify the dynamics of nanoscale particles over a broad range of concentrations.

Department of Chemical and Biomolecular Engineering, University of Houston, Houston, TX 77204-4004, USA. E-mail: ramanan@uh.edu; jcconrad@uh.edu

† Electronic supplementary information (ESI) available. See DOI: 10.1039/c2sm26392k

2. Experimental methods

2.1 Materials

Fluoro-Max Dyed Red Aqueous Fluorescent polystyrene particles with diameters (d_p) of 100 nm, 200 nm and 400 nm were purchased from Thermo Fisher Scientific. The polymer matrix in these cross-linked polystyrene nanoparticles is saturated with fluorescent dye, thereby rendering the nanoparticles uniformly bright. The nanoparticles are well dispersed in water with the aid of trace amounts of surfactant to inhibit aggregation and promote stability at a weight fraction of 1%. The nanoparticles have a density of 1.05 g cm^{-3} and a refractive index of 1.59 at a wavelength of 589 nm (25 °C). The peak excitation and peak emission wavelengths are 542 nm and 612 nm, respectively (ESI, Fig. S1†).

2.2 Sample preparation

Samples for both DLS and DDM experiments were prepared by diluting dispersions of nanoparticles from master batches of 1 wt% nanoparticles with deuterium oxide (Sigma-Aldrich) that was filtered through a 0.2 μm polyethersulfone syringe filter. To minimize contamination, filtered D_2O was first added to a 20 ml disposable vial that was repeatedly rinsed with deionized water and then dried in a heated convection oven. Nanoparticle dispersions (1 wt%) were then added to the D_2O using a pipette. Following this protocol, dispersions with volume fractions of nanoparticles ranging from $\varphi = 1 \times 10^{-3}$ (corresponding to number densities of 1.8×10^{12} ml^{-1}, 2.2×10^{11} ml^{-1} and 2.8×10^{10} ml^{-1} for 100 nm, 200 nm, and 400 nm nanoparticles, respectively) to 1×10^{-6} (corresponding to number densities of 1.8×10^{9} ml^{-1}, 2.2×10^{8} ml^{-1} and 2.8×10^{7} ml^{-1} for 100, 200, and 400 nm nanoparticles, respectively) were prepared. To minimize the effects of aggregation and ensure uniform dispersal of nanoparticles, all samples were sonicated for 15 s in a low power ultrasonic bath prior to each measurement.

2.3 Dynamic light scattering

Light scattering data were collected on a Brookhaven Instruments goniometer (BI-200SM, Brookhaven Instruments Corporation) equipped with a highly sensitive avalanche photodiode detector (Brookhaven, BI-APD), a sample cell assembly (including a filtration circulation system for the index matching liquid (BI-FC), a temperature controller (BI-TCD), a sample filtration system that cleans the light scattering samples (BI-SFS) and a sample holder), a digital correlator (Brookhaven, TurboCorr) that calculates the photon intensity autocorrelation function, and a Mini-L30 laser (wavelength $\lambda = 637.6$ nm). To minimize scattering due to contaminants or dirt in the optics, all sample vials were carefully rinsed with soapy water and then cleaned with acetone and lens paper prior to insertion in the DLS sample holder. We collected the scattered light at a fixed scattering angle θ for 15 s and repeated this measurement 20 times to obtain an average intensity–intensity correlation function $g^2(q,\tau) = \langle I(t)I(t+\tau)\rangle/\langle I(t)\rangle^2$ at 400 delay times ranging between 0.5 μs and 2 s.

To determine the diffusion coefficient of the nanoparticles from the DLS measurements, we first fitted the second-order autocorrelation function $g^2(q,\tau)$ to the Siegert equation,[3]

$$g^2(q,\tau) = 1 + \beta g^1(q,\tau) \quad (1)$$

and obtained the first-order autocorrelation function $g^1(q,\tau)$; here β is the correction parameter depending on the laser-beam geometry and alignment in the light scattering setup and is close to unity. We then obtained the photon correlation relaxation time Γ by assuming that the first-order autocorrelation function could be described by a single-exponential decay:

$$g^1(q,\tau) = \exp(-\Gamma\tau) \quad (2)$$

and calculated the diffusion coefficient D_m as:

$$D_m = \Gamma/q^2 \quad (3)$$

where q is the scattering vector and is equal to $4\pi n/\lambda(\sin\theta/2)$, n is the index of refraction of the solvent ($n = 1.328$ for D_2O) and $\lambda = 637.6$ nm is the wavelength of the incident laser light. We performed DLS measurements at four different scattering angles (30°, 45°, 60°, and 90°, corresponding to scattering wave vectors $q = 6.8$ μm^{-1}, 10.1 μm^{-1}, 13.2 μm^{-1} and 18.6 μm^{-1} respectively) to provide independent verification of the DDM measured diffusion coefficients.

2.4 Differential dynamic microscopy

Samples for differential dynamic microscopy were sealed in glass chambers constructed from cover glasses (ESI, Fig. S2†). Two 22 mm × 22 mm cover glasses (thickness 0.19–0.23 mm, Fisherbrand) were attached using an epoxy-based adhesive (Devcon) to a rectangular cover glass with dimensions of 48 mm × 65 mm (thickness 0.13–0.17 mm, Gold Seal). A 22 mm × 22 mm cover glass was then centered on top of the two cover glasses to create an open chamber. One of the two openings of the chamber was sealed with epoxy, and nanoparticle dispersions were introduced into the chamber through the other opening, which was subsequently sealed with epoxy to form a hermetic glass chamber.

Nanoparticle dispersions were imaged on a Leica DM4000 inverted microscope with a 100× oil immersion objective (Leica Microsystems HCX PL APO, numerical aperture of 1.40) and a pixel size of 0.195 ± 0.002 μm per pixel using a high speed AOS Camera (AOS Technologies AG). An optional 1.6× lens was added to the imaging train to improve the pixel resolution to 0.124 ± 0.001 μm per pixel. For brightfield DDM measurements, a condenser (numerical aperture 0.7) was used. For the fluorescence DDM measurements, a "k" filter cube N2.1 Green (excitation – band pass 515–560 nm, dichroic reflection short pass (D-RKP580), barrier filter – long pass 590 nm) was used to capture only the fluorescence emitted from the nanoparticles. In a typical experiment, we collected 4200 images of size 640 pixels × 480 pixels at a frame rate of 63 or 120 frames per second under either fluorescence or brightfield modes.

To extract the dynamics of nanoparticle diffusion from the time-dependent microscopy images, we implemented a DDM algorithm for both brightfield DDM (b-DDM) and fluorescence DDM (f-DDM) micrographs as described in the literature.[16,17]

We first subtracted two images that were separated by a fixed delay time Δt to eliminate the time-invariant background and thereby obtained the intensity difference $D(x,y;\Delta t) = I(x,y;t + \Delta t) - I(x,y;t)$. Here, $I(x,y;t)$ is the intensity at position (x,y) measured at time t, and the delay-time Δt ranges from a minimum value of 0.0083 or 0.0158 s to a maximum value of 13 or 25 s for images captured at 120 and 63 frames per second, respectively. The physical significance of $D(x,y;\Delta t)$ depends on the particle size: for particles whose diameters fall below the resolution limit of the microscope, image subtraction generated a speckle pattern similar to that obtained in DLS, whereas for larger particles image subtraction is directly related to the density fluctuations. We then calculated the 2D fast Fourier transform (FFT) of $D(x,y;\Delta t)$, and obtained the Fourier power spectrum $D(u_x,u_y;\Delta t)$ by averaging over all image pairs, *i.e.* $D(u_x,u_y;\Delta t) = \langle|\Delta\hat{I}(u_x,u_y;\Delta t)|^2\rangle$, where (u_x,u_y) are the coordinates in Fourier space. To ensure that adequate statistics were obtained for each value of the delay-time, we averaged the signal from 1700–n image pairs at each Δt (n = frame rate × Δt); this process ensured that a minimum of 100 image pairs were averaged even for the largest value of delay-time investigated (*i.e.*, $n = 1600$). Assuming that the sample was isotropic, the 2-D power spectrum was azimuthally averaged to obtain the one-dimensional power spectrum or image structure function $D(q,\Delta t)$,[17] where $q = 2\pi\sqrt{u_x^2 + u_y^2}$ is the scattering wavevector. We fitted the image structure function data to

$$D(q,\Delta t) = A(q)\left[1 - \exp\left(-\frac{\Delta t}{\tau(q)}\right)\right] + B(q) \quad (4)$$

and extracted three parameters: the signal prefactor $A(q)$, the background $B(q)$, and the q-dependent relaxation time $\tau(q)$. A detailed derivation of eqn (4) was given in ref. 14 and 16. On the basis of the development in ref. 16, eqn (4) is valid for imaging processes that are linear space invariant, *i.e.*, when the intensity is directly proportional to the density of particles, as holds for both brightfield and fluorescence microscopy. Notably, the validity of eqn (4) does not depend on the size of the particles or on the physical process by which the structure function is generated. Non-linear least-squares fitting was performed using the Levenberg–Marquardt algorithm as implemented in Origin® (OriginLab, Northampton, MA). Finally, we calculated the particle diffusivity D_m from the slope of $\tau(q)$ *versus* q^2 as $D_m = 1/\tau(q)q^2$. Errors in the diffusion coefficient were estimated by evaluating systematic and stochastic errors associated with the collection of the time dependence of the structure function data and with their fitting to deduce the diffusion coefficient.

The q-range over which structure data were collected was dictated by the optical elements of the microscopy apparatus. The minimum accessible scattering wavevector $q_{min} = 2\pi/L$ is inversely proportional to the largest dimension of the image L, which for a particular camera is dictated by the objective lens used. The maximum wavevector q_{max} accessible in these measurements is determined by the smallest resolvable distance that a particle travels between two successive images and is estimated as $(q_{max})^2$ = frame rate/D_m, using the diffusion coefficient D_m measured from DLS measurements. Table 1 lists the accessible range of q in the experiments performed in this study. In practice, we find that the effective value of q_{min} is ~0.5 μm^{-1} irrespective of the objective lens used because of the limitation imposed by the length of the movies that could be recorded and analyzed: for values of $q \lesssim 0.5$ μm^{-1} the dynamics of decorrelation for all the nanoparticle dispersions studied here were sufficiently slow such that we did not observe the final plateau corresponding to complete decorrelation.

Table 1 Minimum and maximum values of the scattering wavevector q (q_{min} and q_{max}, respectively) that can be accessed in the DDM measurements described here

Objective	q_{min} (μm^{-1})		
160×	0.11		
100×	0.07		
Video capture rate	q_{max} (μm^{-1})		
Frame rate (fps)	d_p = 100 nm	d_p = 200 nm	d_p = 400 nm
120	5.58	7.72	11.33
63	4.05	5.59	8.21

3. Results and discussion

We collected time-resolved brightfield and fluorescence optical micrographs for nanoparticle dispersions in D_2O with the particle volume fraction, φ, ranging from 10^{-6} to 10^{-3}. Typical brightfield and fluorescence microscopy images for 100 nm and 400 nm diameter nanoparticles at $\varphi = 10^{-3}$ are shown in Fig. 1. For the 400 nm particles, we are able to detect individual nanoparticles with both brightfield and fluorescence microscopy. By contrast, for the 100 nm particles, whose diameter is smaller than the resolution limit of the microscope, a diffuse speckle pattern is observed using both brightfield and fluorescence microscopy. The large dark spots visible in all images are dust

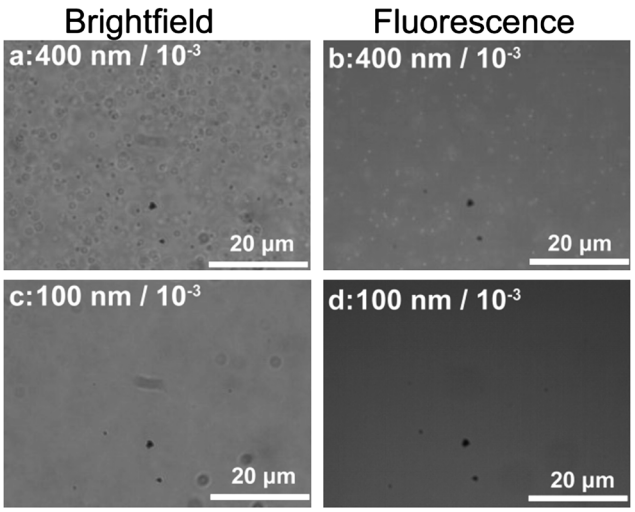

Fig. 1 Brightfield (a and c) and fluorescence (b and d) micrographs of an aqueous (D_2O) dispersion of 400 nm diameter nanoparticles (a and b) and 100 nm diameter nanoparticles (c and d) at a particle volume fraction φ of 10^{-3} corresponding to number densities of 2.8×10^{10} ml^{-1} and 1.8×10^{12} ml^{-1}, respectively. While the larger 400 nm particles can be individually resolved in the images, the 100 nm particles cannot be individually resolved.

particles that adhere to the camera or to other optical elements of the microscope. The time-independent background subtraction described in the Experimental methods to obtain the differential images removed these time-invariant features observed in the micrographs, and therefore the DDM measurements did not require specially prepared and cleaned optical elements.

From a time series of images similar to those shown in Fig. 1, we calculated the delay-time dependence of the image structure function $D(q,\Delta t)$. Representative delay-time dependence of $D(q,\Delta t)$ obtained using b-DDM (left) and f-DDM (right) at four values of q (=1.9 μm^{-1}, 2.67 μm^{-1}, 3.45 μm^{-1} and 5 μm^{-1}) for dispersions of nanoparticles with diameter 100, 200, or 400 nm is shown in Fig. 2. Data at different values of q and nanoparticle sizes, $D(q,\Delta t)$ increased monotonically with the delay-time Δt until it reached a plateau at long delay-times, indicating that the system had become decorrelated. The delay-time dependence of the increase in the scattering or fluorescence signal is controlled by the time required for the particles to diffuse a distance $2\pi/q$, resulting in the sigmoidal shaped plots of $D(q,\Delta t)$ as a function of Δt and a characteristic time scale associated with this sigmoidal dependence that increases with decreasing q-value. Notably, the data for $D(q,\Delta t)$ obtained on a dispersion of 100 nm nanoparticles at $q = 5$ μm^{-1} using f-DDM (Fig. 2f) do not exhibit the expected sigmoidal dependence and cannot be fit to eqn (4). This reflects the fundamental limitation imposed by the camera frame rate on q_{max} and is not a limitation of the method in general: for the frame rate used for these experiments (63 fps), $q = 5$ μm^{-1} lies outside the range of $q = 0.07$–4.05 μm^{-1} that can be investigated.

The delay-time dependence of the structure function data was fitted to eqn (4) to extract the signal prefactor $A(q)$, the background term $B(q)$ and the relaxation time $\tau(q)$.[16,17] We note that the background term $B(q)$ contains information that is only dependent on the optics of the microscope. Therefore, at low concentrations of the nanoparticles $B(q)$ is related only to the power-spectrum of the optical train in the microscope.[16] Representative fit parameters $A(q)$ and $B(q)$ for a dispersion of 400 nm diameter nanoparticles with volume fraction $\varphi = 10^{-4}$ are shown in Fig. 3. The background term $B(q)$ is nearly constant over the range of q investigated for both b-DDM and f-DDM and increases slightly at the lowest values of q, which may indicate some long-wavelength heterogeneity in the optical elements. Moreover, at low concentrations ($\varphi = 10^{-5}$, 10^{-6}) we find that $B(q)$ is largely independent of the concentration and diameter of the nanoparticles (ESI, Fig. S3 and S4†), consistent with the notion that $B(q)$ is a function of the experimental setup alone and with previous studies in the literature. We use this fact to extract dynamical information from structure functions in which the short-time plateau is not clearly resolved (*e.g.*, for 100 nm particles or large wavevectors, as shown in Fig. 2). Specifically, we use these concentration and particle size independent values of $B(q)$ as the initial guess to fit the structure function data for these cases. For concentrated samples ($\varphi = 10^{-4}$, 10^{-3}), because the magnitude of the signal prefactor $A(q)$ was significantly larger than that of the background term $B(q)$, the relaxation time $\tau(q)$ obtained using a best fit value of $B(q)$ or setting $B(q) = 0$ was identical within the errors of the measurements. These protocols allowed us to obtain robust fits to the structure functions across the investigated range of concentrations, wavevectors and particle sizes.

The behavior of the signal prefactor term $A(q)$ is different in b-DDM and f-DDM: in b-DDM $A(q)$ exhibits a local maximum at $q = 1$ μm^{-1}, whereas in f-DDM $A(q)$ decreases monotonically with increasing q (Fig. 3). This prefactor term is associated with the q-dependent loss of coherence and is strongly dependent on the wave-vector cut-off associated with the type of microscopy. The observed trends in $A(q)$ are consistent with previous reports and represent the differences in the loss of coherence in brightfield and fluorescence imaging used here.

The third q-dependent parameter obtained by fitting the structure function data to eqn (4) is the relaxation time $\tau(q)$, as shown for representative data for 400 nm dispersions in Fig. 4. Over three orders of magnitude in volume fraction

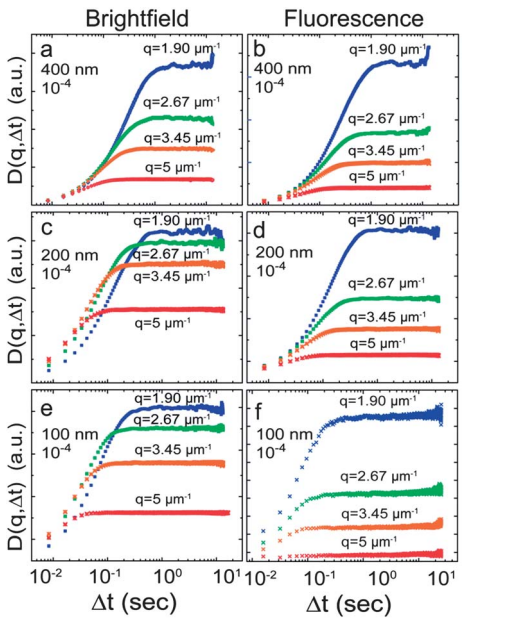

Fig. 2 Structure function $D(q,\Delta t)$ as a function of time delay Δt at wavevectors q of 1.9 μm^{-1} (blue), 2.67 μm^{-1} (green), 3.45 μm^{-1} (orange), and 5 μm^{-1} (red) calculated using the brightfield DDM (b-DDM, a, c and e) and fluorescence DDM (f-DDM, b, d and f) for 400 nm diameter nanoparticles (a and b); 200 nm nanoparticles (c and d); and 100 nm nanoparticles (e and f). The nanoparticle volume fraction $\varphi = 10^{-4}$ for all measurements is shown here.

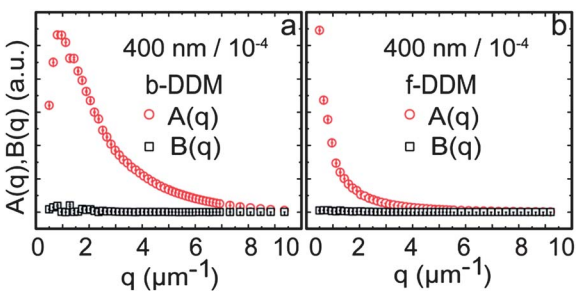

Fig. 3 Fitting parameters $A(q)$ (red circles) and $B(q)$ (black squares) as a function of wave vector q obtained by fitting the (a) b-DDM and (b) f-DDM data to eqn (4). Data shown here correspond to fitted parameters obtained for an aqueous dispersion of 400 nm nanoparticles at a volume fraction of 10^{-4}. The error bars for both $A(q)$ and $B(q)$ are smaller than the symbols.

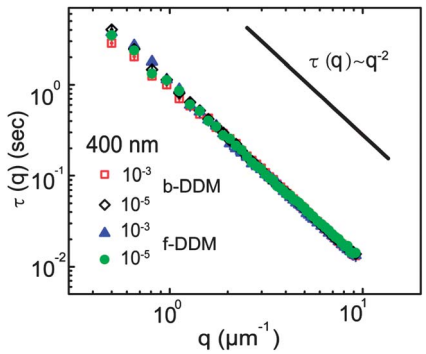

Fig. 4 Relaxation time $\tau(q)$ as a function of wave vector q (μm^{-1}) obtained by fitting the b-DDM (open symbols) and f-DDM (filled symbols) structure functions to eqn (4) for an aqueous dispersion of 400 nm nanoparticles at volume fractions of 10^{-3} and 10^{-5}. The relaxation time $\tau(q)$ scales as q^{-2} as expected from the anticipated free diffusive behavior of the nanoparticles. The error bars for $\tau(q)$ are smaller than the symbols.

($\varphi = 10^{-3}$ to 10^{-6}) and over one order of magnitude in wavevector q, $\tau(q)$ scales as q^{-2} as expected for freely diffusing nanoparticles in solution. Similarly, for the case of dispersions of 100 and 200 nm diameter nanoparticles, we find good agreement with the behavior expected on the basis of the diffusive dynamics of individual nanoparticles over a wide range of volume fractions. Furthermore, we obtain excellent agreement between f-DDM and b-DDM measurements, demonstrating that the linear space-invariant images provided by fluorescence microscopy can also be used to extract dynamic information that is similar to that obtained from brightfield microscopy.[16]

We further confirm that the relaxation times measured by DDM (both brightfield and fluorescence) reflect free diffusion by measuring the relaxation times at larger wavevectors using dynamic light scattering (DLS). Across nearly two orders of magnitude in q, the $\tau(q) \sim q^{-2}$ scaling is maintained for all particle dispersions, as shown in Fig. 5. Moreover, the values of $\tau(q)$ obtained from the DDM measurements quantitatively extrapolate to those obtained from the DLS measurements at higher q-values.

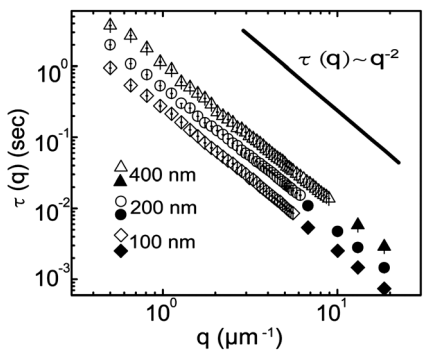

Fig. 5 Relaxation time $\tau(q)$ (in seconds) as a function of wavevector q (in μm^{-1}) for aqueous dispersions of 100 nm (diamonds), 200 nm (circles), and 400 nm (triangles) nanoparticles from DDM and DLS measurements. Open symbols correspond to DDM measurements and filled symbols correspond to DLS measurements. The relaxation times $\tau(q)$ obtained from DDM extrapolate quantitatively to the data obtained from DLS measurements, which demonstrates their equivalence.

The values of the diffusion coefficients for nanoparticles of various diameters over a wide range of dispersion concentrations using b-DDM, f-DDM and DLS are summarized in Table 2. Over three orders of magnitude in volume fraction (10^{-3} to 10^{-6}) of 100 to 400 nm nanoparticles, the diffusion coefficients measured using the three techniques are in excellent agreement within experimental errors. Moreover, we have shown that f-DDM can be used to measure diffusion coefficients for nanoparticles whose size is smaller than the optical resolution of the microscope, and have extended the range of accessible volume fractions down to 10^{-6}. A second advantage of the two DDM techniques is that they can access smaller scattering vectors as compared to those accessed with conventional DLS and therefore can be used to probe longer length (and time) scale dynamics. Finally, we note that DDM accurately measures the diffusion coefficient at larger volume fractions ($\varphi = 10^{-3}$) where multiple scattering precludes DLS measurements. These features make DDM an excellent and versatile technique to complement DLS measurements, and will enable optical methods to be extended to quantify the diffusion of nanoparticles in complex geometries and complex media.

We have identified two different scenarios where the DDM methodology does not provide accurate data for the dynamics of nanoparticles. First, as either the concentration of nanoparticles or their size is decreased, the ratio of the signal term $A(q)$ to the background term $B(q)$ decreases. This leads to significant errors in the fitting of the structure function data (obtained in either b-DDM or f-DDM) to eqn (4) and therefore in the estimation of the associated characteristic relaxation time scale. Importantly, the values of $\tau(q)$ typically do not scale as q^{-2}, and therefore the diffusion coefficients deduced from these measurements are inherently unreliable. Empirically, we found that limiting the data to those cases where the ratio $A(q)/B(q)$ was greater than 0.07 for f-DDM or greater than 0.2 for b-DDM yielded diffusion coefficients that were generally reliable. Secondly, for the smallest nanoparticles considered here under highly dilute conditions, the structure function measured with f-DDM does not exhibit an exponential increase (shown for a sample with $\varphi = 10^{-5}$ in the ESI, Fig. S8†) and cannot be fitted using eqn (4).

Table 2 Diffusion coefficients (in $\mu m^2\ s^{-1}$) measured using b-DDM, f-DDM and DLS for aqueous dispersions of nanoparticles at 25 °C

NP diameter	Volume fraction, φ	Diffusion coefficient ($\mu m^2\ s^{-1}$) b-DDM	f-DDM	DLS
400 nm	1×10^{-3}	0.96 ± 0.06	0.95 ± 0.04	—
	1×10^{-4}	0.94 ± 0.05	0.95 ± 0.06	—
	1×10^{-5}	0.95 ± 0.03	0.94 ± 0.05	0.92 ± 0.06
	1×10^{-6}	0.93 ± 0.02	0.96 ± 0.06	0.97 ± 0.05
200 nm	1×10^{-3}	1.88 ± 0.10	1.89 ± 0.10	—
	1×10^{-4}	1.89 ± 0.12	1.92 ± 0.10	—
	1×10^{-5}	1.92 ± 0.06	1.92 ± 0.11	2.01 ± 0.06
	1×10^{-6}	1.93 ± 0.07	1.89 ± 0.27	2.01 ± 0.05
100 nm	1×10^{-3}	3.83 ± 0.11	3.91 ± 0.14	—
	1×10^{-4}	3.79 ± 0.09	3.71 ± 0.20	—
	1×10^{-5}	3.60 ± 0.14	Immeasurable	3.83 ± 0.06
	1×10^{-6}	3.60 ± 0.34	Immeasurable	3.87 ± 0.09

For these samples the signal from f-DDM is extremely weak due to the small number of fluorescent particles and the low fluorescence associated with each nanoparticle and therefore the decorrelation cannot be observed beyond the background noise. Despite these limitations that result from weak signals in dilute suspensions, we found that the two DDM methods are quite powerful and vastly expand the use of optical methods to characterize the mobility of nanoparticles in confined and complex media.

4. Concluding remarks

In conclusion, there is excellent agreement between the diffusion coefficients obtained for nanoparticles dispersed in water by brightfield and fluorescence based DDM and conventional DLS. We find that the DDM methods are particularly powerful and reliable in systems with high concentrations of particles where traditional DLS methods fail. In addition, the broad range of q-values accessible in DDM methods allows for new investigations of the dynamics of nanoparticle systems over a wide range of length scales. We therefore believe that such DDM based methods, while being particularly useful for studying complex biological systems, are also powerful tools to investigate the dynamics of nano- and micro-particles in complex media, such as those encountered in drug/nutrient delivery in tissue engineering, soil and ground water contamination by nanoparticles and to sub-surface applications for improved hydrocarbon exploration and production.

Note added after first publication

This article replaces the version published on 4th October 2012, which contained errors in the author affiliations (email addresses missing).

Acknowledgements

We thank Prof. J. Rimer for the use of the DLS instrumentation. This publication is based on the work supported in part by award no. KUS-C1-018-02, made by King Abdullah University of Science and Technology (KAUST).

References

1 B. Godin, E. Tasciotti, X. W. Liu, R. E. Serda and M. Ferrari, *Acc. Chem. Res.*, 2011, **44**, 979–989.
2 J. R. Lead and K. J. Wilkinson, *Environ. Chem.*, 2006, **3**, 159–171.
3 B. J. Berne and R. Pecora, *Dynamic Light Scattering: With Applications to Chemistry, Biology and Physics*, 2000.
4 T. Thurn-Albrecht, G. Meier, P. Muller-Buschbaum, A. Patkowski, W. Steffen, G. Grubel, D. L. Abernathy, O. Diat, M. Winter, M. G. Koch and M. T. Reetz, *Phys. Rev. E: Stat. Phys., Plasmas, Fluids, Relat. Interdiscip. Top.*, 1999, **59**, 642–649.
5 V. V. Nesvizhevsky, *Phys. At. Nucl.*, 2002, **65**, 400–408.
6 J. C. Crocker and D. G. Grier, *J. Colloid Interface Sci.*, 1996, **179**, 298–310.
7 R. Dzakpasu and D. Axelrod, *Biophys. J.*, 2004, **87**, 1279–1287.
8 R. Dzakpasu and D. Axelrod, *Biophys. J.*, 2004, **87**, 1288–1297.
9 P. Habdas and E. R. Weeks, *Curr. Opin. Colloid Interface Sci.*, 2002, **7**, 196–203.
10 R. Besseling, L. Isa, E. R. Weeks and W. C. K. Poon, *Adv. Colloid Interface Sci.*, 2009, **146**, 1–17.
11 M. C. Jenkins and S. U. Egelhaaf, *Adv. Colloid Interface Sci.*, 2008, **136**, 65–92.
12 R. Cerbino and V. Trappe, *Phys. Rev. Lett.*, 2008, **100**, 188102.
13 R. Cerbino and A. Vailati, *Curr. Opin. Colloid Interface Sci.*, 2009, **14**, 416–425.
14 L. G. Wilson, V. A. Martinez, J. Schwarz-Linek, J. Tailleur, G. Bryant, P. N. Pusey and W. C. K. Poon, *Phys. Rev. Lett.*, 2011, **106**, 018101.
15 M. Reufer, V. A. Martinez, P. Schurtenberger and W. C. K. Poon, *Langmuir*, 2012, **28**, 4618–4624.
16 F. Giavazzi, D. Brogioli, V. Trappe, T. Bellini and R. Cerbino, *Phys. Rev. E: Stat., Nonlinear, Soft Matter Phys.*, 2009, **80**, 031403.
17 P. J. Lu, F. Giavazzi, T. E. Angelini, E. Zaccarelli, F. Jargstorff, A. B. Schofield, J. N. Wilking, M. B. Romanowsky, D. A. Weitz and R. Cerbino, *Phys. Rev. Lett.*, 2012, **108**, 218103.